

Jintao LIANG, Zhengfeng MING, Peida LI

System construction of a four-side primary permanent-magnet linear motor drive mechanical press

© Higher Education Press 2020

Abstract A primary permanent-magnet linear motor (PPMLM) has a robust secondary structure and high force density and is appropriate for direct-drive mechanical press. The structure of a four-side PPMLM drive press is presented based on our previous research. The entire press control system is constructed to realize various flexible forming processes. The control system scheme is determined in accordance with the mathematical model of PPMLM, and active disturbance rejection control is implemented in the servo controller. Field-circuit coupling simulation is applied to estimate the system's performance. Then, a press prototype with 6 kN nominal force is fabricated, and the hardware platform of the control system is constructed for experimental study. Punch strokes with 0.06 m displacement are implemented at trapezoidal speeds of 0.1 and 0.2 m/s; the dynamic position tracking errors are less than 0.45 and 0.82 mm, respectively. Afterward, continuous reciprocating strokes are performed, and the positioning errors at the bottom dead center are less than 0.015 mm. Complex pulse trajectories are also achieved. The proposed PPMLM drive press exhibits a fast dynamic response and favorable tracking precision and is suitable for various forming processes.

Keywords mechanical press, direct drive, primary permanent-magnet linear motor (PPMLM), servo system, active disturbance rejection control (ADRC), prototype experiment

1 Introduction

Mechanical press is a widely used equipment in metal forming [1]. Owing to the elimination of linear motion

conversion mechanisms, such as crank link and ball screw, a press that is directly driven by a permanent-magnet linear motor (PMLM) exhibits a compact structure, high transmission efficiency, high positioning precision, and fast dynamic response. Reference [2] summarized several linear drive applications of metal-forming machines. The drawback of traditional PMLM drive is that either the permanent magnets (PMs) or the coils are installed on the slider (mover) [3,4]; thus, good protection and heat dissipation are required, and the fabrication cost is high. Primary permanent-magnet linear motor (PPMLM) is a novel PMLM wherein the PMs and coils are arranged on the primary side, and the secondary side contains only the salient pole core [5–8]; it is robust against impact loading. Our research group has developed several PPMLM direct-drive apparatuses in recent years [9].

A linear-drive mechanical press features controllable force in the entire punching stroke, and various punch trajectories can be achieved for a flexible forming process [10–12]. However, various parameter variations and external disturbances directly affect the linear motor. In particular, the forming resistance is high, and the friction force is unknown [13–15]. Therefore, a matching servo control system should be developed with the novel PPMLM drive press to obtain fast dynamic responses, high positioning precision, and strong disturbance rejection.

The complete servo control system of a novel four-side PPMLM drive mechanical press is presented in this paper. The press structure and electromagnetic characteristics of the PPMLM are introduced based on our previous research [16], and the control model is established. The drive scheme is also determined, and common field-oriented control (FOC) is utilized in the current loop. Moreover, active disturbance rejection control (ADRC) [17,18] is applied in the servo control loop. ADRC involves the use of a proportional–derivative (PD) controller to implement position tracking control, a linear extended state observer (LESO) to estimate system lumped disturbance, and a feedforward controller to improve the dynamic response.

Received November 2, 2019; accepted June 8, 2020

Jintao LIANG (✉), Zhengfeng MING, Peida LI
School of Mechano-Electronic Engineering, Xidian University, Xi'an 710071, China
E-mail: jtliang@xidian.edu.cn

Field-circuit coupling simulation is conducted to evaluate the system characteristics. For an experimental study, a 6 kN press prototype is manufactured, and the servo control system is implemented. Punch strokes with different speeds and trajectories are tested, and the results exhibit favorable dynamic tracking and static positioning performance.

2 PPMLM drive mechanical press

2.1 Machine structure

A four-side PPMLM drive mechanical press is designed based on our previous research and shown in Fig. 1. Four symmetrical PPMLMs are arranged around the punch synchronously to balance the normal force between the primary and the secondary. The three-phase, short-primary/long-secondary topology of PPMLM is utilized. The multi-tooth primary core modules and PMs are arranged alternately on each primary, and the end PMs are employed on both margins to compensate for the longitudinal end effect. Three-phase interval windings are wound around two adjacent primary core modules. Correspondingly, each secondary module contains only the salient pole core, which is directly installed on the punch. In addition, a pneumatic cylinder is used to generate pneumatic force for balancing the punch weight. Hence, the punch transmission has a compact structure,

strong robustness, and low inertia and is suitable for realizing various flexible forming processes.

2.2 PPMLM characteristics

The three-phase, no-load electromotive force (EMF) waveforms are obtained through an electromagnetic finite element analysis (FEA) of the PPMLM and shown in Fig. 2(a). The waveforms exhibit a sinusoidal characteristic. Electromagnetic force is generated when three-phase sinusoidal current with the same phase difference as EMF is injected to the three-phase windings. The rated current is set to 15.7 A, and the rated force is about 1500 N, as shown in Fig. 2(b). The output force increases as the input current increases, as shown in Fig. 2(c). The force–current ratio is called force coefficient k_f . Saturation becomes serious when the current is more than two times the rated value; thus, the maximum phase current is set to 31.4 A. The four PPMLMs drive the punch synchronously, and the windings of the same phase in each PPMLM can be connected in series or in parallel, as shown in Fig. 3. The series–parallel connection is selected in consideration of inverter selection and fault tolerance.

2.3 Mathematical model

A mathematical model of the four-side PPMLM drive press should be established for control system construction. In accordance with the three-phase circuit, the phase

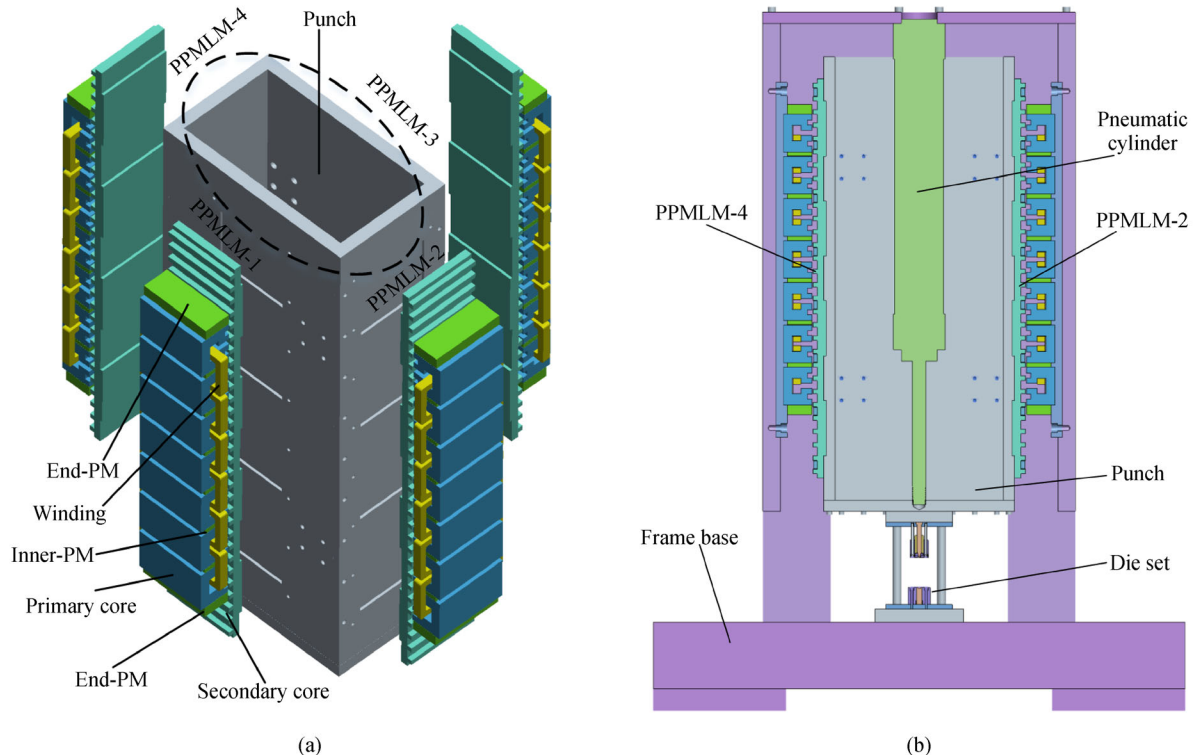


Fig. 1 Structure of the four-side PPMLM drive press: (a) Magnified view and (b) front sectional view.

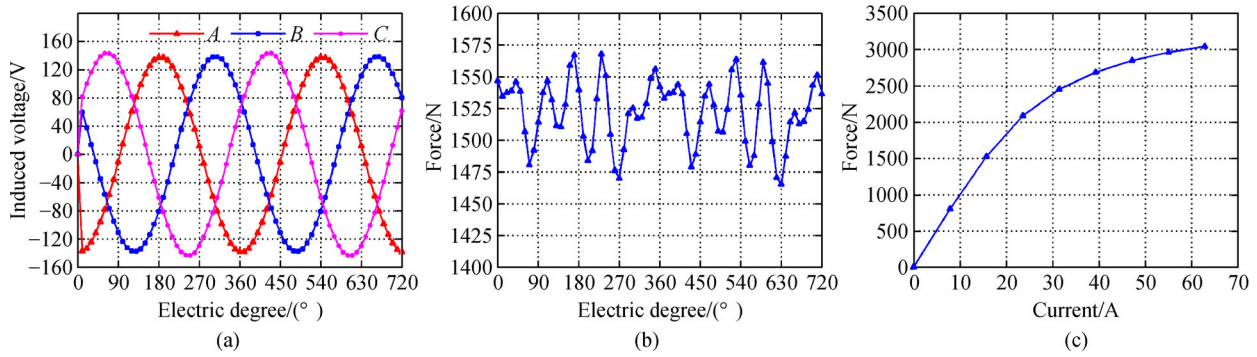


Fig. 2 Electromagnetic characteristics of PPMLM: (a) No-load EMF, (b) electromagnetic force, (c) force–current ratio.

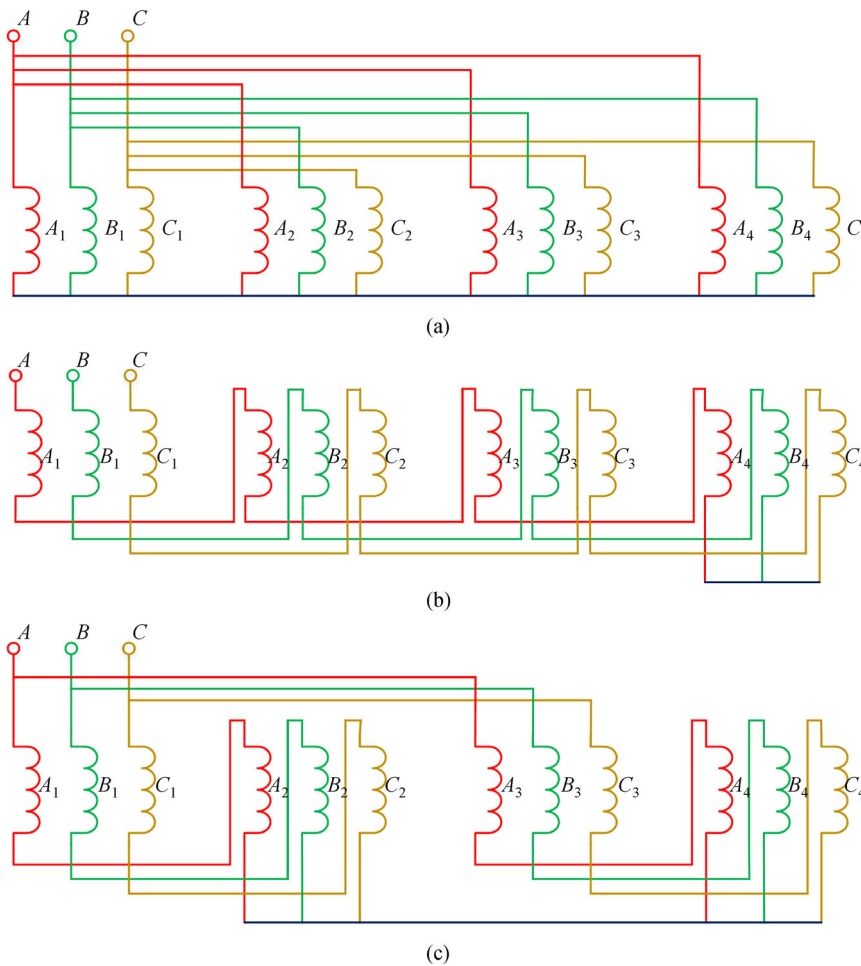


Fig. 3 Winding connection of the four PPMLMs: (a) Parallel connection, (b) series connection, and (c) series–parallel connection.

voltage equation is expressed as

$$\begin{bmatrix} u_A \\ u_B \\ u_C \end{bmatrix} = \begin{bmatrix} R & 0 & 0 \\ 0 & R & 0 \\ 0 & 0 & R \end{bmatrix} \times \begin{bmatrix} i_A \\ i_B \\ i_C \end{bmatrix} + \frac{d}{dt} \begin{bmatrix} \psi_A \\ \psi_B \\ \psi_C \end{bmatrix}, \quad (1)$$

where $u_A, u_B, u_C, i_A, i_B,$ and i_C pertain to three-phase ABC

voltage and current, R is the phase resistance, and $\psi_A, \psi_B,$ and ψ_C are the three-phase flux linkage.

PPMLM exhibits sinusoidal characteristics that are similar to those of common PMLMs [19–21]. Thus, the three phase vectors can be decoupled into d – q coordinate vectors via Clarke and Park transformation, and the voltage equation can be changed to

$$\begin{cases} u_d = L_d \frac{di_d}{dt} - \frac{2\pi v}{\tau_s} L_q i_q + R i_d, \\ u_q = L_q \frac{di_q}{dt} + \frac{2\pi v}{\tau_s} (L_d i_d + \psi_{pm}) + R i_q, \end{cases} \quad (2)$$

where u_d , u_q , i_d , and i_q denote the transformed d - and q -axis voltage and current, respectively, L_d and L_q are the d - and q -axis inductance, respectively, ψ_{pm} is the flux linkage generated by the PMS, p_s and τ_s are the pole pairs and pole pitch of the secondary, respectively, and v is the speed of the secondary (punch). In accordance with the output power, the electromagnetic force of PPMLM (F_e) is expressed as

$$F_e = \frac{3\pi}{\tau_s} [\psi_{pm} i_q + (L_d - L_q) i_d i_q] \approx \frac{3\pi}{\tau_s} \psi_{pm} i_q \approx k_f i_q. \quad (3)$$

The reluctance force can be disregarded because the proposed PPMLM has a multi-pole/tooth topology, and the difference between L_d and L_q is small. The “ $i_d=0$ ” of FOC method is applied, and F_e is mainly determined by i_q .

The following motion equation is established through force analysis of the punch.

$$m \frac{d^2 x}{dt^2} = k_f i_q - k_d \frac{dx}{dt} + mg - F_p - F_l - F_f, \quad (4)$$

where x is the punch displacement, m is the mass of the entire punch, k_d is the damping coefficient, F_p is the pneumatic force supplied by the pneumatic cylinder, F_l is the load force, and F_f is the frictional resistance. In practice, k_f and m can be estimated and measured approximately, but their values may change. F_p is regulated to balance punch gravity mg , but it changes with cylinder pressure. In addition, k_d , F_l , and F_f are difficult to calculate.

For a linear drive system, these parameter variations and external disturbances affect drive performance. The motion equation is expressed as

$$\begin{aligned} & (m_0 + \Delta m) \frac{d^2 x}{dt^2} \\ &= -k_d \frac{dx}{dt} + (k_{f0} + \Delta k_f) i_q + (m_0 g - F_l - F_p - F_f), \end{aligned} \quad (5)$$

where m_0 and k_{f0} are the estimated values of the corresponding parameters, and Δm and Δk_f are uncertain variations. All system uncertainty can be lumped as σ_u as follows:

$$\sigma_u = - \left(\Delta m \frac{d^2 x}{dt^2} + k_d \frac{dx}{dt} - \Delta k_f i_q - m_0 g + F_l + F_p + F_f \right) / m_0. \quad (6)$$

Then, the motion equation can be simplified as

$$\frac{d^2 x}{dt^2} = b_0 i_q + \sigma_u, \quad (7)$$

where $b_0 = k_{f0}/m_0$.

3 Servo control system

3.1 System composition

The control scheme established in accordance with the PPMLM characteristics and model is shown in Fig. 4. PPMLM power is supplied by three-phase rectifier and inverter circuits, and the input current can be controlled using vector transformation and pulse width modulation (PWM) algorithms to track the servo controller command

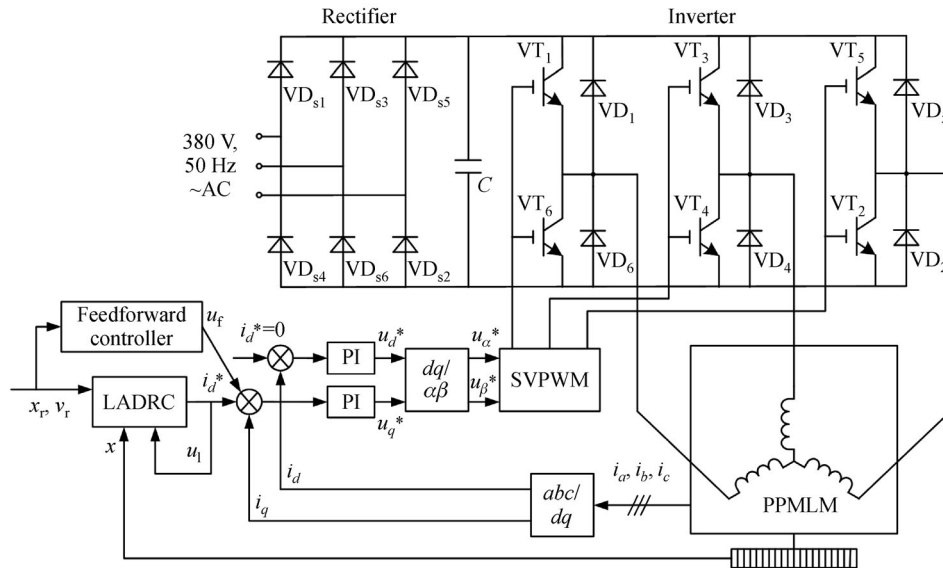


Fig. 4 Schematic of the entire drive system.

i_q^* . In the servo control loop, a linear ADRC algorithm is applied to implement the trajectory command. A linear feedforward (FF) controller is also used to improve the dynamic response performance when necessary, u_f is the output of the FF.

3.2 Linear active disturbance rejection control

ADRC was proposed by the Chinese scholar Jingqing Han in 1999 and has been widely applied in various fields [22–25]. ADRC is mainly composed of a tracking differentiator for transient profile generation, an extended state observer (ESO) for comprehensive disturbance estimation and compensation, and a nonlinear state error feedback for control. On this basis, Gao [18] utilized a linear function to simplify ADRC. This linear ADRC (LADRC), which reduces system calculation and parameter turning, is easy to apply in actual engineering. On the basis of Eq. (7), LADRC is used as the position servo controller to construct the proposed press system. A schematic of LADRC is shown in Fig. 5. The trajectory position and speed are the input commands, and a PD controller is used to implement tracking control. An LESO is also utilized to estimate the press system's extended states, namely, punch position, speed, and lumped disturbance.

The discrete state equation of LESO is expressed as

$$\begin{cases} \mathbf{z}(k+1) = \mathbf{F}_E \times \mathbf{z}(k) + \mathbf{G}_E \times \mathbf{u}_d(k), \\ \mathbf{y}_d(k) = \mathbf{H}_E \times \mathbf{z}(k) + \mathbf{J}_E \times \mathbf{u}_d(k), \end{cases} \quad (8)$$

where $\mathbf{z}(k) = [z_1(k), z_2(k), z_3(k)]^T$ is the state vector of LESO, $\mathbf{u}_d(k) = [u_1(k), x(k)]^T$ is the LESO input vector, $u_1(k)$ is the control effort of LADRC, and $x(k)$ is the measured punch displacement, as shown in Fig. 5. $\mathbf{y}_d(k) = [y_1(k), y_2(k), y_3(k)]^T$ is the ESO output vector, that is, $y_1(k)$, $y_2(k)$, and $y_3(k)$ are the three estimated variables corresponding to punch system disperse state variables, the punch displacement $x(k)$, the punch speed $v(k)$, and the lumped uncertainty $\sigma_u(k)$, respectively.

\mathbf{F}_E , \mathbf{G}_E , \mathbf{H}_E , and \mathbf{J}_E are the coefficient matrixes of LESO and given as follows:

$$\begin{cases} \mathbf{F}_E = \begin{bmatrix} 3\beta-2 & h & h^2/2 \\ -(1-\beta)^2(5+\beta)/(2h) & 1 & h \\ -(1-\beta)^3/h^2 & 0 & 1 \end{bmatrix}, \\ \mathbf{G}_E = \begin{bmatrix} b_0 h^2/2 & 3-3\beta \\ b_0 h & (1-\beta)^2(5+\beta)/(2h) \\ 0 & (1-\beta)^3/h^2 \end{bmatrix}, \\ \mathbf{H}_E = \begin{bmatrix} \beta^3 & 0 & 0 \\ -3(1-\beta)^2(1+\beta)/(2h) & 1 & 0 \\ -(1-\beta)^3/h^2 & 0 & 1 \end{bmatrix}, \\ \mathbf{J}_E = \begin{bmatrix} 0 & 1-\beta^3 \\ 0 & 3(1-\beta)^2(1+\beta)/(2h) \\ 0 & (1-\beta)^3/h^2 \end{bmatrix}, \end{cases} \quad (9)$$

where β is the bandwidth of discrete LESO and h is the sampling period. The output variables of LESO, namely, $y_1(k)$, $y_2(k)$, and $y_3(k)$, can be calculated as

$$\begin{cases} y_1(k) = \beta^3 z_1(k) + (1-\beta^3)x(k), \\ y_2(k) = -3z_1(k)(1-\beta)^2(1+\beta)/(2h) + z_2(k) \\ \quad + 3x(k)(1-\beta)^2(1+\beta)/(2h), \\ y_3(k) = -z_1(k)(1-\beta)^3/h^2 + z_3(k) + x(k)(1-\beta)^3/h^2. \end{cases} \quad (10)$$

LESO output variables $y_1(k)$ and $y_2(k)$ are used as position and speed feedback, respectively. $y_3(k)$ is used to compensate for the lumped disturbance. Correspondingly, the PD controller is defined as

$$u_1(k) = \frac{1}{b_0} \{k_p [x_r(k) - y_1(k)] + k_d [v_r(k) - y_2(k)] - y_3(k)\}, \quad (11)$$

where $x_r(k)$ and $v_r(k)$ are the disperse displacement and speed reference commands, respectively, k_p and k_d are

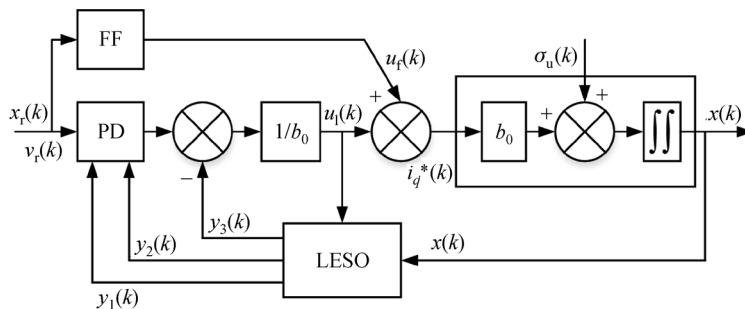


Fig. 5 Schematic of a linear active disturbance rejection control.

proportional and differential coefficients, respectively, and can be determined by controller bandwidth b_w as follows:

$$k_p = b_w^2, \quad k_d = 2b_w. \quad (12)$$

Thus, in the entire LADRC, only four parameters (h , b_0 , β , and b_w) need to be determined. h is determined by the system hardware capability, and b_0 can be calculated using the FEA model and approximately verified by the experiment results. In reference to previous research, the bandwidth relationship can be regulated within a certain range, as follows:

$$\beta = e^{kb_w h}, \quad k = 2, 3, \dots, 10. \quad (13)$$

3.3 Field-circuit coupling simulation

System simulation is usually performed for the estimation of dynamic characteristics. Conventional simulation implemented in Simulink with a mathematical model does not consider nonlinear factors, such as saturation, leakage flux, and harmonic component in the magnetic field. Therefore, field-circuit coupling analysis of the entire drive system is conducted. Instead of a mathematical model, the FEA model of PPMLM is established using Maxwell. The power electric circuit is built with Simplorer. A 540 V DC voltage source is used instead of the three-phase 380 V AC source and rectifier, and the three-phase insulated gate bipolar translator (IGBT) inverter is connected to the FEA model. The proposed servo controller and current control loop are operated in Simulink. Through exchange interfaces, the motor status variables (actual displacement x , speed v , electromagnetic force F_e , and three-phase current i_A , i_B , and i_C) are obtained from the FEA model, and the PWM drive control signals are sent back to the six IGBTs. Furthermore, the loading condition is set and connected to the FEA model in Simplorer.

The common quadratic displacement trajectory with trapezoidal speed is simulated. The displacement is set to 0.09 m, and the constant speed value is 0.3 m/s. The constant resistance is assumed to be 500 N, and a loading

disturbance of 300 N is added between 0.24 and 0.26 s. In LADRC, only four control parameters should be regulated during the trial. These parameters are $\beta = 0.8$, $b_0 = 2/3$, $k_p = 1000000$, and $k_d = 2000$. A proportion–integration–differentiation (PID) controller is also used for comparison. The simulation results are shown in Fig. 6.

The speed waveforms show that LADRC exhibits good anti-disturbance capability, and its tracking error is small. When the load suddenly increases, a slight speed drop occurs, but the system recovers immediately. The speed drop is less than 3%, and the recovery time is about 50 ms. The observed disturbance value, y_3 , compensates for the input resistance, and the PPMLM presents a sufficiently fast force response. However, under the large time interval setting, the output force of the FEA model exhibits a large ripple, which is the main reason the speed drop and ripple are slightly large.

4 Press prototype and system platform

For an experimental study, a 6 kN prototype of the proposed four-side PPMLM drive mechanical press is built and shown in Fig. 7. The uniform rated force of each PPMLM is 1500 N, and the rated speed is 1.2 m/s. The number of turns of each phase is 120, and each winding is wound by a double-strand enameled wire with a 1 mm diameter. The rated phase current is set to 31.4 A for the series–parallel connection. The maximum stroke of the punch is set to 0.12 m. A grating sensor (Renishaw RGS40-S/RH100X30D05A) is used to measure the punch's real-time position, and the resolution is 1 $\mu\text{m}/\text{pulse}$. The weight of the punch is about 150 kg, and a pneumatic cylinder with 100 mm diameter is utilized to export the pressure for balancing the punch weight. The pressure is supplied and controlled by a compressor and a gasholder, and the maximum pressure is 0.7 MPa.

The hardware platform of the control system, which includes a personal computer (PC), motion controller, and AC amplifier, is built and shown in Fig. 8. The human–machine interface (HMI) of the press system is developed on the PC. Through HMI, the trajectory command is sent

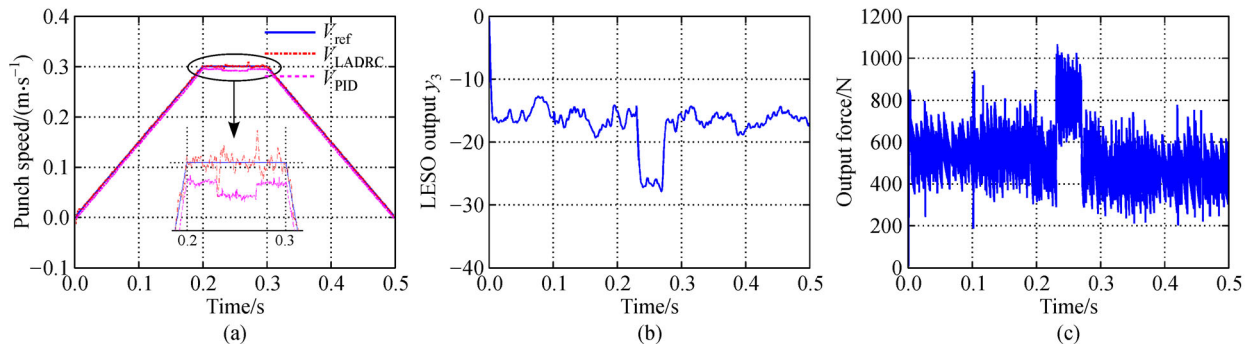


Fig. 6 Field-circuit coupling simulation results. (a) Punch speed, (b) LESO output y_3 , and (c) output force.

to the motion controller, and the system feedback information is collected and displayed in real time. The servo control algorithm LADRC is programmed in the motion controller to generate the q -axis current control command. Then, the current command is sent to the AC amplifier to implement current control and drive the PPMLM.

5 Experiment study

The drive performance is experimentally studied before actual forming processes are implemented on the proposed press system. The quadratic trajectory is tested with a reciprocating stroke of 0.06 m and different trapezoidal speeds of 0.1 and 0.2 m/s. The experiment results, including speed, position, and i_q current waveforms, are shown in Fig. 9.

Although the punch weight is large, the initial response is sufficiently fast. The dynamic speed ripple is slightly large in the 0.1 m/s trapezoidal waveform, but it becomes

small in the 0.2 m/s trapezoidal waveform. The ripple at a constant speed 0.2 m/s is about 0.005 m/s; the dynamic position tracking errors are less than 0.45 and 0.82 mm, respectively, indicating that the servo control performance is favorable. Given that the prototype is built for the first time, the machining and assembling precision are insufficient and thus affect the drive performance considerably. After manufacturing improvement, the speed ripple and positioning error decrease effectively. The force on the punch can be analyzed using the I_q and three-phase current waveforms shown in Fig. 10.

The punch stroke can be divided into upward and downward stages. Given that the cylinder cannot easily adjust pneumatic force F_p to balance punch gravity mg completely, the difference $(F_p - mg)$ directly affects the PPMLM input current. The current in the upward stage is larger than that in the downward stage, indicating that the direction of $(F_p - mg)$ is downward. Therefore, the accelerating current in the upward stage is larger than the decelerating current; in the downward stage, the

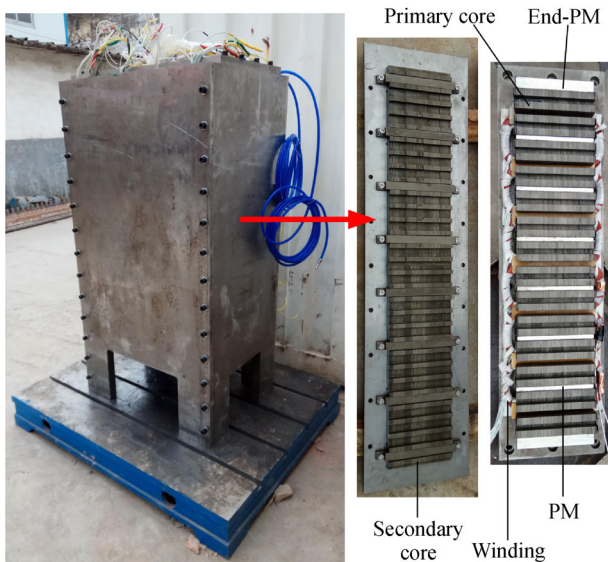


Fig. 7 6 kN prototype of the four-side PPMLM drive press.

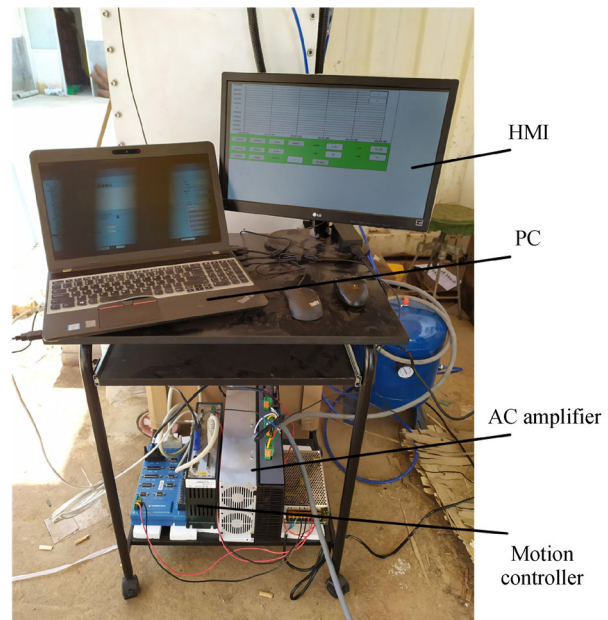


Fig. 8 Servo control system of the four-side PPMLM drive press.

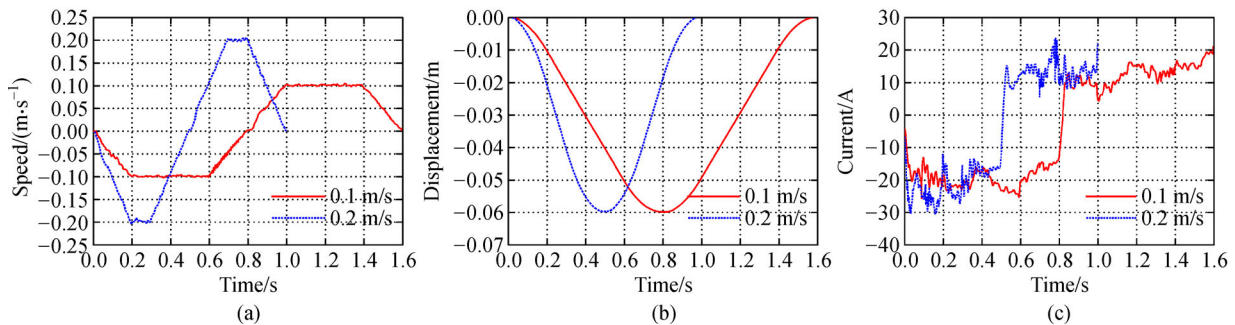


Fig. 9 60 mm stroke achievement with different speeds. (a) Speed waveforms, (b) position waveforms, and (c) I_q current waveforms.

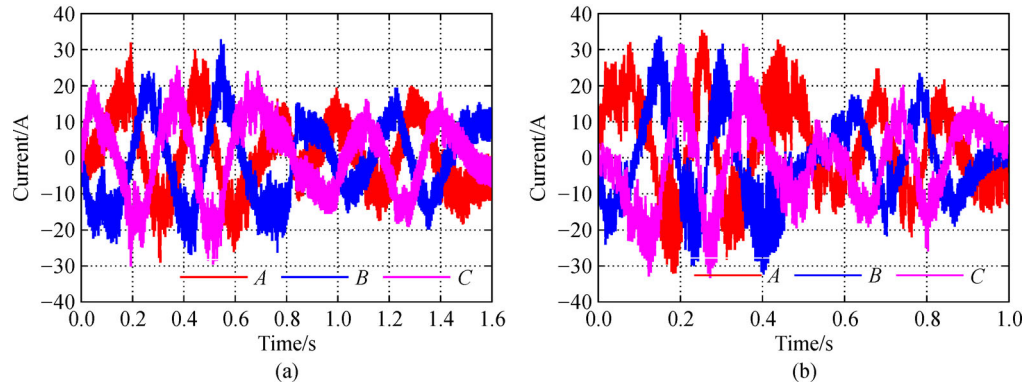


Fig. 10 Current waveforms of one stroke with different speeds: (a) 0.1 and (b) 0.2 m/s.

accelerating current is lower than the decelerating current. Moreover, viscous friction, sliding damping, and other disturbance resistances influence the PPMLM force/current characteristics.

In practice, mechanical presses always implement a repetitive forming process for high productivity. The continuous operation performance of the proposed system is determined. Ten reciprocating strokes with trapezoidal speed 0.1 and 0.2 m/s waveforms are implemented, and the operating trajectories are shown in Fig. 11. For the 10 strokes, the positioning errors at the bottom dead center are less than 0.015 mm, indicating that continuous forming processes can be implemented precisely. Furthermore, continuous operation increases the PPMLM temperature, which influences drive performance considerably. Therefore, the thermal performance of the proposed system is further investigated under continuous processing.

The drive performance of the advance pulse trajectory is tested to determine the capacity of the proposed press system for complicated process achievement. Four-time 20 mm and seven-time 10 mm advance pulse trajectories are implemented, and the operating trajectories are shown in Fig. 12. The punch displacement in the proposed drive press can be controlled flexibly, and the dynamic response

is good. Compared with a traditional mechanical press, the proposed PPMLM drive press can implement various flexible forming processes more easily.

6 Conclusions

A four-side PPMLM drive mechanical press system is presented in this paper. The linear direct drive electro-mechanical structure is introduced, and the electromagnetic characteristic is analyzed with the FEA model. On the basis of the PPMLM mathematical model, “ $i_d = 0$ ” of FOC is used in the current loop. LADRC is employed in the servo control loop for a fast dynamic response and robust tracking performance. A 6 kN prototype of the proposed press is manufactured, and a complete servo control system is established for an experimental study. Quadratic and advance pulse trajectories are implemented, and the results show that the dynamic tracking performance is favorable. Moreover, continuous reciprocating strokes are implemented, and the positioning error between strokes is sufficiently small. Therefore, the proposed servo press system can be applied in various metal forming processes, such as metal sheet blanking, drawing, and jointing.

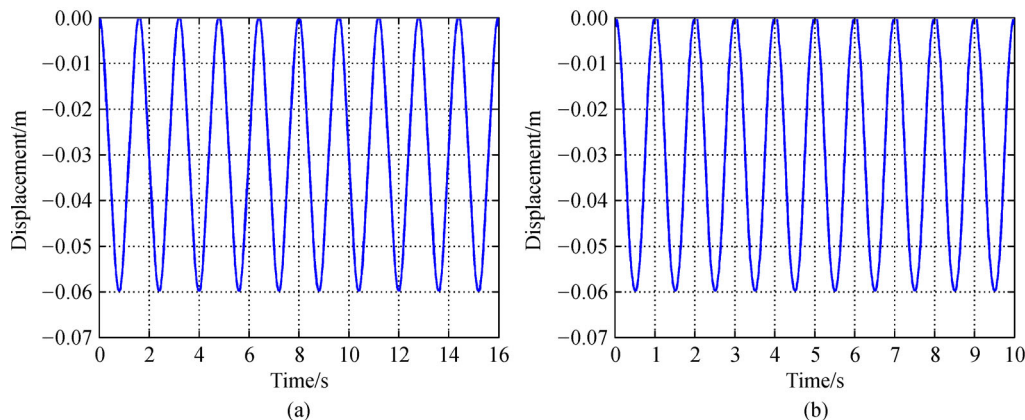


Fig. 11 Ten continuous strokes achieved with different speeds. Trapezoidal speed of (a) 0.1 and (b) 0.2 m/s.

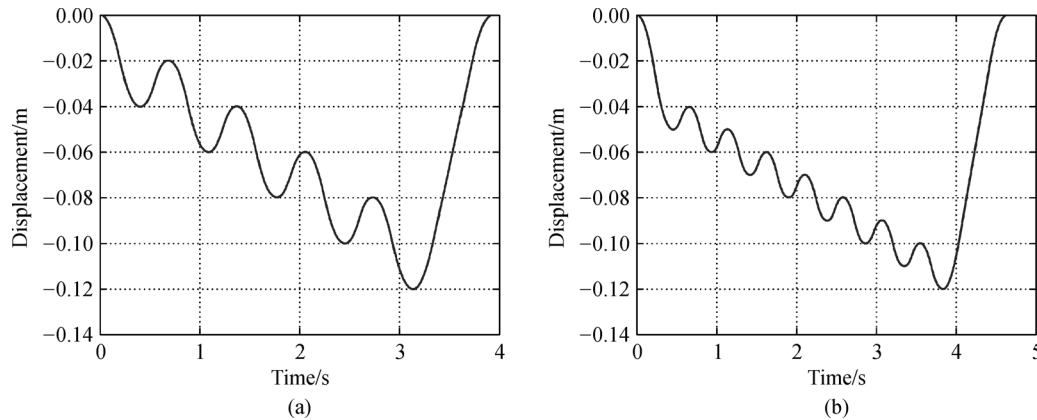


Fig. 12 Advance pulse trajectory achievement: (a) Four-time 20 mm and (b) seven-time 10 mm pulse waveform.

Acknowledgements This research was financially supported by the National Natural Science Foundation of China (Grant No. 51605363), China Postdoctoral Science Foundation (Grant No. 2016M590922), and Shaanxi Postdoctoral Research Project Funding.

Electronic Supplementary Material The supplementary material can be found in the online version of this article at <https://doi.org/10.1007/s11465-020-0597-z> and is accessible to authorized users.

References

- Osakada K, Mori K, Altan T, et al. Mechanical servo press technology for metal forming. *CIRP Annals*, 2011, 60(2): 651–672
- Behrens B A, Krimm R, Reich D, et al. Linear drives in metal forming machines and peripherals-recent developments. *Journal of Manufacturing Processes*, 2016, 22: 192–198
- Xu J, Guo B, Shan D B, et al. Development of a micro-forming system for micro-punching process of micro-hole arrays in brass foil. *Journal of Materials Processing Technology*, 2012, 212(11): 2238–2246
- Sato K. High-precision and high-speed positioning of 100 G linear synchronous motor. *Precision Engineering*, 2015, 39: 31–37
- Nasiri-Gheidari Z, Tootoonchian F. Electromagnetic design optimization of a modular linear flux-reversal motor. *Electric Power Components and Systems*, 2016, 44(18): 2112–2120
- Zeng Z Q, Lu Q F. Investigation of novel partitioned-primary hybrid-excited flux-switching linear machines. *IEEE Transactions on Industrial Electronics*, 2018, 65(12): 9804–9813
- Ullah N, Basit A, Khan F, et al. Enhancing capabilities of double sided linear flux switching permanent magnet machines. *Energies*, 2018, 11(10): 2781
- Chung S U, Kim J W, Woo B C, et al. Design and experimental validation of doubly salient permanent magnet linear synchronous motor for precision position control. *Mechatronics*, 2013, 23(2): 172–181
- Liang J T, Ming Z F. Servo X-Y biaxial feed system of flux switching permanent magnet linear motor. *Review of Scientific Instruments*, 2019, 90(7): 074703
- Nakagava T, Higuchi T, Sato R, et al. Linear motor drive CNC press using learning control. *CIRP Annals*, 1999, 48(1): 199–202
- Matsumoto R, Hayashi K, Utsunomiya H. Experimental and numerical analysis of friction in high aspect ratio combined forward-backward extrusion with retreat and advance pulse ram motion on a servo press. *Journal of Materials Processing Technology*, 2014, 214(4): 936–944
- Jeon J Y, Matsumoto R, Utsunomiya H. Two-step die motion for die quenching of AA2024 aluminum alloy billet on servo press. *Materials Transactions*, 2014, 55(5): 818–826
- Matsumoto R, Sawa S, Utsunomiya H, et al. Prevention of galling in forming of deep hole with retreat and advance pulse ram motion on servo press. *CIRP Annals*, 2011, 60(1): 315–318
- Maeno T, Mori K, Hori A. Application of load pulsation using servo press to plate forging of stainless steel parts. *Journal of Materials Processing Technology*, 2014, 214(7): 1379–1387
- Song Q Y, Guo B F, Li J. Drawing motion profile planning and optimizing for heavy servo press. *International Journal of Advanced Manufacturing Technology*, 2013, 69(9–12): 2819–2831
- Liang J T, Ji X P, Gong W J, et al. Design and analysis of a novel stator permanent magnet linear motor drive mechanical press. In: *Proceedings of 2018 IEEE International Conference on Mechatronics and Automation (ICMA)*. Changchun: IEEE, 2018
- Han J Q. From PID to active disturbance rejection control. *IEEE Transactions on Industrial Electronics*, 2009, 56(3): 900–906
- Gao Z Q. On the centrality of disturbance rejection in automatic control. *ISA Transactions*, 2014, 53(4): 850–857
- Tong L, Lin M Y. Study on a high thrust force bi-double-sided permanent magnet linear synchronous motor. *Advances in Mechanical Engineering*, 2016, 8(3): 1–10
- Ting C S, Chang Y N, Shi B W, et al. Adaptive backstepping control for permanent magnet linear synchronous motor servo drive. *IET Electric Power Applications*, 2015, 9(3): 265–279
- Huang W T, Hua W, Yin F B, et al. Model predictive thrust force control of a linear flux-switching permanent magnet machine with voltage vectors selection and synthesis. *IEEE Transactions on Industrial Electronics*, 2019, 66(6): 4956–4967
- Du C, Yin Z G, Zhang Y P, et al. Research on active disturbance rejection control with parameter autotune mechanism for induction

- motors based on adaptive particle swarm optimization algorithm with dynamic inertia weight. *IEEE Transactions on Power Electronics*, 2019, 34(3): 2841–2855
23. Zhang X H, Zhu Q, Sun Y K, et al. Three-degree-of-freedom positioning control of magnetically levitated permanent magnet planar motor using active disturbance rejection control scheme. *Advances in Mechanical Engineering*, 2017, 9(7): 1–13
24. Amjad J H, Ibraheem K I. Speed control of permanent magnet DC motor with friction and measurement noise using novel nonlinear extended using novel nonlinear extended state observer-based anti-disturbance control. *Energies*, 2019, 12(9): 1651
25. Vera-Tizatl P, Luviano-Juarez A, Santos-Cuevas L, et al. Tracking control of tomographic image acquisition robotic system based on active disturbance rejection theory with adaptive gains. *Proceedings of the Institution of Mechanical Engineers, Part I: Journal of Systems and Control Engineering*, 2020, 234(1): 81–95